PCCP

PAPER

Cite this: *Phys. Chem. Chem. Phys.*, 2015, **17**, 32316

Suspensions of carbon nanofibers in organic medium: rheo-electrical properties†

Mohamed Youssry,*[a] Dominique Guyomard[b] and Bernard Lestriez[b]

Received 17th October 2015,
Accepted 7th November 2015

DOI: 10.1039/c5cp06303e

www.rsc.org/pccp

The nonaqueous suspensions of carbon nanofibers (CNFs) in 1 M lithium bis(trifluoromethanesulfonaimide) in propylene carbonate electrolyte reveal unique structural evolution and shear-induced transition due to the high aspect ratio. The rheo-electrical behavior elucidates a microstructural transition from entangled-to-aggregated networks above a distinct percolation threshold. Under shear flow, both networks show a three-regime flow curve and an inverted-bell-like conductivity curve as a consequence of shear-induced alignment (entangled network) and shear-induced breaking up (aggregated network). The different particle morphology of carbon nanofibers (anisometric) and carbon black (CB; isometric) causes different aggregation mechanisms (aggregate *vs.* particulate) and then varied microstructure for their suspensions in the same electrolyte. This fact explains the higher rigidity and lower electric conductivity of CNFs than CB suspensions. Interestingly, the suspension of hybrid carbons at the optimum mixing ratio merges the advantages of both carbons to operate efficiently as precursors in the formulation of electrodes for energy storage systems.

1. Introduction

Carbon nanofibers (CNFs) are special kinds of carbonaceous nanomaterials which have been widely used as conductive fillers in the formulations of electrodes for energy storage systems such as ion-batteries[1–6] and electrochemical capacitors,[7] due to their unique chemical, mechanical, and electrical properties. They resemble carbon nanotubes (CNTs) where both nanomaterials are formed from graphite sheets with sp^2 hybridized carbon atoms arranged in a cylindrical structure, while the sheets are stacked with an angle to the fiber axis (not parallel) resulting in exposed edge planes on the interior and exterior surfaces of the nanofibers.[8] According to the feedstock, synthesis route and conditions, CNFs have a wide range of aspect ratios (length/diameter >100) with an average diameter of 50–200 nm and length scale of several tens of μm.[9] Such high aspect ratios and strong van der Waals attraction forces result in aggregation (bundling) of nanofibers and formation of larger agglomerates so that flocculated suspensions are formed especially at higher CNF concentrations in polar solvents, similar to CNT suspensions.[10] The electric current only flows on the outermost fibers in bundled CNFs, while the inner fibers do not contribute significantly to the current[11] resulting in potential loss of electronic wiring. To overcome the dominant van der Waals forces, many approaches, including the physical adsorption of amphiphiles[12,13] and chemical functionalization,[14,15] have been developed and stable dispersions of such filamentous materials (CNTs or CNFs) have been obtained. However, these methods seriously disrupt the graphitic structure of the sidewall[16] and reduce the aspect ratio[17] of nanofibers/nanotubes resulting in a significant change in the electrical conductivity of suspensions. Moreover, the colloidal stability of the suspensions becomes out of control when the nanofibers/nanotubes entangle and then percolate far above a critical concentration, the so-called percolation threshold (ϕ^*; ϕ denotes the volume fraction of carbon materials). Above this threshold, a two- or three-dimensional network of nanofibers/nanotubes is formed which is signified by an abrupt change in the rheological parameters (plateau modulus G_0 or yield stress σ_y)[18] when the infinite network is constructed. This is called the rheological percolation threshold (ϕ_r^*). On the other hand, the electrical percolation threshold (ϕ_e^*) is characterized by a sudden increase in the electrical conductivity (Σ) when the conductive pathways are formed across the suspension. Usually, the rheological and electrical thresholds slightly differ and in some cases coincide depending on the state of dispersion, particle orientation and size distribution.[19,20] In general, even a small infinite cluster is required to reach the electrical threshold; however, the rheological threshold appears when a three-dimensional rigid network is fully formed.[20]

In comparison to low-aspect-ratio (nearly isometric) particles such as carbon blacks (CBs), anisometric particles such as CNTs

[a] *Department of Chemistry and Earth Sciences, College of Arts and Sciences, Qatar University, 2713 Doha, Qatar. E-mail: myoussry@qu.edu.qa*
[b] *Institut des Matériaux Jean Rouxel, CNRS, Université de Nantes, 44322 Nantes Cedex 3, France*

† Electronic supplementary information (ESI) available. See DOI: 10.1039/c5cp06303e

and CNFs are expected to: (i) reach the percolation thresholds at concentrations lower than those of isometric particles such as carbon blacks (CBs),[19,21] (ii) have different agglomeration mechanisms, and (iii) respond differently to shear flow. For instance, it is known that the percolating network of aggregated suspension of CBs suffers shear-induced transition under simple shear flow as a consequence of the breaking up of aggregates into smaller flocs.[5] Owing to their higher aspect ratio and flexibility, nanofibers are likely to resist the breaking up of the network, to some extent, so that conductive clusters exist yet.

Carbonaceous materials such as carbon nanofibers are essential conductive components in electrode formulation for battery applications. In order to improve the energy density of batteries, the amount of active material (which is electrically insulator) should be increased. This increase breaks up the electrically percolating network resulting in the loss of electrical pathways.[6,22] Besides their excellent electrical properties, the filamentous morphology and flexibility of carbon nanofibers adapt them to be used as a conductive component which sustains higher loading of active materials and shear-induced breaking up of their network. Vapor grown carbon fibers are special types of carbon fibers which are characterized by large surface area, small diameter, high mechanical strength, electrical conductivity, and unique network-like morphology; thus they showed improved performance in the electrodes of lithium-ion batteries.[3]

In this work, we have systematically studied the flow-structure relationship in suspensions of carbon nanofibers in an organic electrolyte (1 M lithium bis(trifluoromethanesulfonaimide) in propylene carbonate) for redox-flow batteries at 25 °C. Under the same conditions, the effect of particle morphology (isotropic carbon black *vs.* anisometric carbon nanofiber) on the equilibrium agglomeration mechanism and shear-induced transition is comparatively addressed. In addition, the rheo-electrical behavior of suspensions of mixed carbons (carbon black and nanofibers) is demonstrated in an attempt to find out the optimum composition of conductive suspension as a precursor for electrodes for battery applications.

2. Experimental

2.1. Material and suspension preparation

Carbon nanofibers (CNFs; Vapor-Grown Carbon Fiber-S with an average diameter d = 100 nm, average length L = 10 μm, density = 1.90 g cm^{-3}, and BET surface area = 35 m^2 g^{-1}) and propylene carbonate (PC; 99.7%) were purchased from Showa Denko and Sigma-Aldrich, respectively. Lithium bis(trifluoromethanesulfonaimide) (LiTFSI) was kindly provided by 3 M as a gift.

Using ball-milling (FRITSCH, Planetary Micro Mill PULVERISETTE 7 classic line), the suspensions were prepared by mixing appropriate amounts of CNF with solution of 1 M LiTFSI in propylene carbonate for 3 h at the ambient temperature. As recommended by FRITSCH, 12 mL grinding bowls were used to commonly prepare 5 mL suspensions. This preparation method yielded homogeneous suspensions with reproducible data.

2.2. Rheo-electrical measurements

Simultaneous electrochemical impedance spectroscopy (EIS) measurements under shear flow were conducted in a stress-controlled rheometer Physica MCR 101 (Anton Paar) equipped with a steel plate–plate geometry (plate diameter 50 mm, gap 1 mm) connected with a standard potentiostat/galvanostat (SP200 from Biologic, France). The plate–plate gap was 1 mm; hundred times larger than the fiber length to eliminate any effect of measurement boundaries.[23]

After loading the suspensions, the shear history was removed by preshearing the samples at 1000 s^{-1} for 10 min and left at rest for 1 h before sweeping the shear rate. At each shear rate, the rheological and electrical data were collected after 30–60 min, depending on the shear rate, where the steady state conditions were attained. The EIS spectra were recorded over a frequency range of 10^{-2}–10^{5} Hz at 25 °C with an alternating current amplitude of 100 mV.

In this study, the electronic conductivity (Σ) values have been obtained by fitting the impedance spectra (see Nyquist plots; Fig. 5) of the samples to an equivalent circuit proposed in our previous study[5] and EC-Labs software (Bio-Logic Science-Instruments). The migration of the ions is described by an ionic resistor associated in series with a capacitive element to take into account the accumulation of ions at the surface of the electrodes compensating their polarization, known as the double-layer. The circulation of the electrons through the percolating network of CB is described by a pure electronic resistance R_e in parallel with the ionic branch.

2.3. Electron microscopy

A scanning electronic microscope (SEM) JEOL JSM 7600F equipped with an energy-dispersive X-ray (EDX) analyzer, operating in secondary electron (SEI) mode, was used to collect the samples' micrographs. After sample preparation, suspension was placed on the sample holder and left to dry before coating with a thin layer of platinum. On the other hand, the morphology of the carbon nanofibers was investigated by transmission electron microscopy (TEM). The TEM specimen was prepared by dispersing traces of CNF powder in acetone; a drop of dispersion was applied to a grid and then dried in air before TEM experiments.

3. Results and discussion

3.1. Morphology of carbon nanofibers

Generally, vapor grown carbon nanofibers are unique kinds of carbonaceous materials that have high aspect ratios (L/d), with large diameters in between carbon nanotubes and conventional nanofibers.[24] In the current study, we use vapor grown carbon nanofibers with diameter d = 100 nm and average length L = 10 μm, so that the aspect ratio (L/d) = 100. As can be seen from TEM micrographs (Fig. 1a and b), the nanofibers have a tree-ring structure with a hollow core and semispherical tip. Moreover, the nanofibers contain bends and other curvatures, and some have a bamboo-like structure with the distance between joints of about 500 nm. Most of the nanofibers are not perfectly

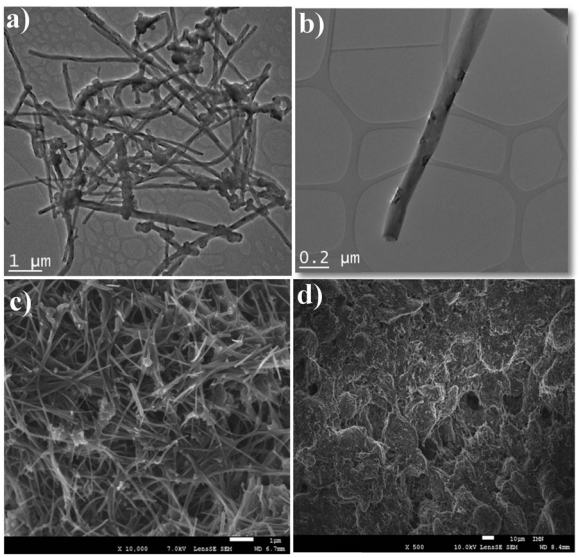

Fig. 1 TEM (a and b) and SEM (c and d) micrographs of CNFs (the bars in micrographs c and d correspond to 1 and 10 μm, respectively).

straight, leading to structurally weak points, *i.e.* more flexible nanofibers. The SEM micrographs represent the microstructure of the suspension of CNFs in propylene carbonate (PC) in the presence of LiTFSI as a salt. The high-magnification SEM micrograph (Fig. 1c) shows highly entangled nanofibers which are bundled into large aggregates (bundles) of a few tens of μm in diameter (Fig. 1d). The aggregates are linked by nanofibers forming an interconnected three dimensional network (Fig. 1d). This is the role of LiTFSI salt which is likely to electrostatically stabilize the aggregates so that a homogenous distribution of connected bundles is formed when compared to the salt-free suspension which shows relatively large isolated bundles (Fig. S1 in the ESI†).

3.2. Nonlinear viscoelasticity of CNF suspensions

Beside its usage to define the linear viscoelastic regime, strain sweep measurement is used to explore the flow behavior of suspensions under large deformation. For some selected suspensions, Fig. 2a shows the strain sweep curves; variation of the elastic (G') and viscous (G'') moduli as functions of the maximum applied oscillatory strain (γ). Rationally, the magnitude of dynamic moduli monotonically increases with the CNF concentration. At small strains, G' is always higher than G'' and suspensions behave gel-like until a critical strain (γ_c) beyond which the moduli crossover appears then G'' becomes higher than G' where the suspensions are liquid-like. For the diluted suspensions, however, it can be noticed that G'' initially rises and then decreases exhibiting a strain overshoot[25] before the moduli crossover and the suspensions behave strain weakening. Such behavior has been reported previously for soft materials[26] and CNT suspensions[27,28] which was attributed to the formation of a transient weak structure which resists the deformation then breaks up above a critical strain (γ_c).[26]

This strain overshoot diminishes as the CNF concentration increases, and the critical strain shows a concentration dependence

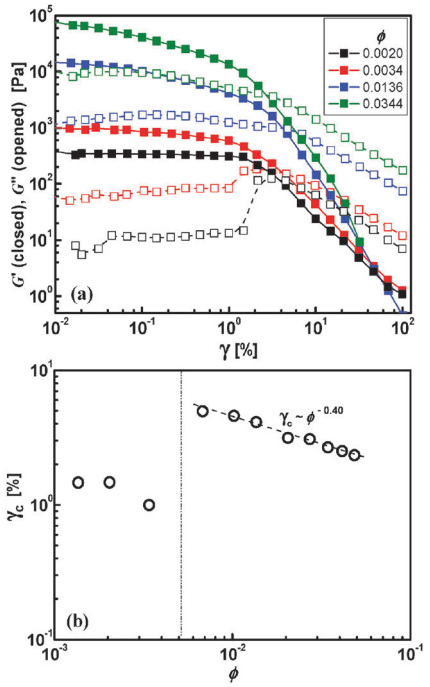

Fig. 2 (a) Strain amplitude dependence (at 1 Hz) of elastic G' (closed) and loss G'' (opened) moduli for some chosen suspensions, and (b) dependence of the critical strain (γ_c) on the nanofiber concentration.

(Fig. 2b) represented by a power law relation with an exponent of -0.4 similar to that exhibited by networks of semiflexible polymers[29,30] and long carbon nanotubes[31] where the deformation is likely attributed to the breaking of bonds between rods and network reorganization.[28,30]

Also, it is worth noting that the γ_c–ϕ curve (Fig. 2b) shows two regimes: at low concentration γ_c is almost independent of ϕ, then shows the power law with a negative exponent (-0.40) at higher concentration. This may imply a structural transition towards rigidly structured suspensions which are more sensitive to the strain as the CNF concentration increases.

3.3. Linear viscoelasticity of CNF suspensions

Insight into the microstructure of CNF suspensions, at equilibrium, can be obtained from the frequency sweep measurements at small deformation in the linear viscoelastic regime in order to guarantee the least disturbance of the internal structures. Dynamic rheological measurements were performed on a wide range of CNF concentration where typical curves of the oscillating frequency dependence of G' and G'' are demonstrated in Fig. 3a. The suspensions exhibit a common gel-like behavior where G' is one-decade higher than G'' and both moduli are nearly independent of the frequency over the entire range. The viscous modulus G'' of the diluted suspension varies slightly with the frequency until G'–G'' crossover appears at higher frequency. This implies the weak gel-like nature of the diluted suspensions. As the CNF concentration increases, the suspensions turn into strong gel-like where the moduli are completely independent of the frequency and hence the moduli crossovers disappear. This viscoelastic behavior denotes strongly

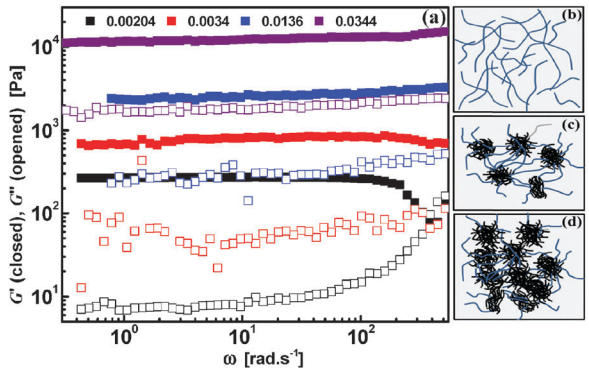

Fig. 3 (a) Dynamic frequency sweep of CNF suspensions at 25 °C. The strain amplitude values, at the linear viscoelastic regimes, were chosen to be 0.3–1% depending on the strain sweep. (b–d) Schematic representation for the possible network structure.

flocculated suspensions with dominant strong irreversible attraction forces (involving energies of several hundreds of kT units).[32] Such behavior has been previously reported for suspensions of spherical carbon black in dispersing medium with poor affinity towards the dispersing particles[5,33,34] and concentrated carbon nanotube suspensions.[27,28,35–37]

For carbon nanotube suspensions, Hough *et al.* attributed the network elasticity to the formation of interconnected networks with bonds that freely rotate and resist stretching.[28] Analogously, it is rational to ascribe the viscoelasticity of the CNF suspensions, at moderate concentration, to the formation of a three-dimensional network formed from aggregates (bundles) held together by freely joined fibers as schematically represented in Fig. 3c and suggested from the SEM micrograph (Fig. 1d). This network becomes densely packed (Fig. 3d) as the volume fraction of the nanofiber increases (as will be described below). For an analogous system (CNF suspension in glycerol/water), Xu *et al.* demonstrated the strong tendency of CNFs to clump into mm-size showing gel-like behavior at higher concentrations.[38]

It is well stated that suspensions of high-aspect-ratio rods are not dilute unless their volume fraction is very low, $\phi \leq (L/d)^{-2}$.[39] Accordingly, it is expected to have CNF suspensions in the semidilute regime at $\phi \geq 0.0001$ (with aspect ratio = 100) if they are well dispersed. This is the behavior of the suspensions at low concentration (ϕ = 0.0014–0.0034) which exhibit a gel-like viscoelastic response with $G' > G''$ in contrast to many colloidal systems that showed a liquid-like response at similar concentrations.[35,37,38,40,41] Such behavior has been reported previously for very dilute CNT suspensions.[27,28] Hough *et al.* reported a rigidity percolation transition in surfactant-stabilized suspensions of single walled CNTs (aspect ratio $\approx$ 150) at ϕ = 0.0026.[28] It is presumably the entangled network of carbon nanofibers (Fig. 3b) that is responsible for such weak gel-like viscoelastic behavior even at very low concentration. Therefore, the microstructural transition and precision determination of thresholds can be followed by examining the variation of the rheological parameters with the concentration of nanofibers.

The plateau modulus (G_0) and yield stress (σ_y) are two important rheological parameters which stand for the network rigidity in terms of number and lifetime of physical bonds between aggregates and the development of network size and compactness. Fig. 4a and b depict the variations of G_0 and σ_y with the volume fraction of nanofibers (ϕ) which are represented by power law relations: $G_0 \sim \phi^m$ and $\sigma_y \sim \phi^n$ with three distinct exponents for m and n correspond to three distinct regimes (Table 1). As mentioned above the diluted suspensions ($\phi \leq 0.0068$) are gel-like viscoelastic with considerable G_0 which shows minor dependence (m = 0.69) of ϕ implying a constant entanglement density of individual nanofibers analogous to semiflexible biopolymers.[43] At $\phi > 0.0068$, G_0 and σ_y steeply increases exhibiting a power law relationship with exponents: m = 2.1 and n = 1.8, respectively. Generally, these exponents are very close to that reported for suspensions of anisometric particles such as CNTs[27,28,31,35,44] and semiflexible biopolymer[29,43] forming a three-dimensional network with bonds resisting stretching and free to rotate.[28] The highly concentrated suspensions ($\phi > 0.034$) show a higher exponent m = 6.3 and n = 6.9, similar to that reported for short single-walled CNTs (aspect ratio = 80) at similar concentration,[31] and multi-walled CNT suspensions in polydimethylsiloxane (aspect ratio = 160).[44]

This behavior is likely to ascribe to a structural transition from an entangled (non-aggregated) network to an aggregate-based network above the rheological percolation threshold (ϕ_r^* = 0.0068).

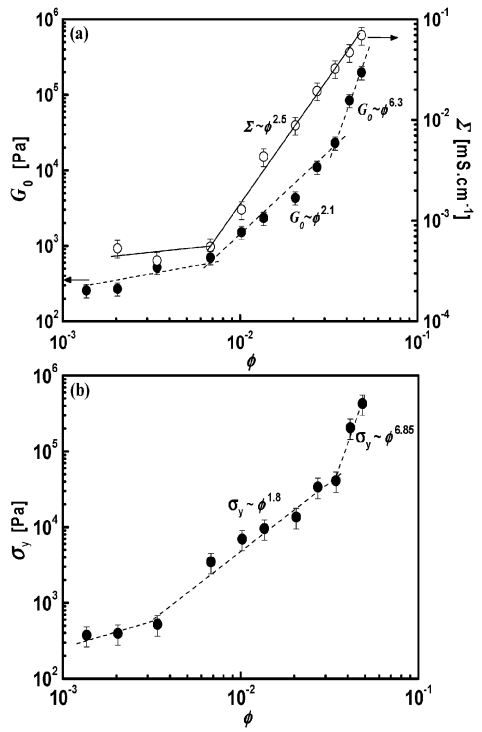

Fig. 4 Variation of (a) the rheological plateau modulus (G_0) and the electric conductivity (Σ), and (b) the yield stress (σ_y) with the concentration of CNFs. The lines are the best fit. The yield stress was calculated using the relation: $\sigma_y = G_0\gamma_c$.[26,42] The electric conductivity was obtained by fitting the impedance spectra to the equivalent circuit (inset of Fig. 5) and substituting R_e in the equation: $R_e = e/\Sigma S$ where e is the thickness of the suspension (gap between upper and lower plates in the rheo-dielectrical cell), and S the plate surface.

Table 1 The evolution of the exponents m (for $G_0 \sim \phi^m$) and n (for $\sigma_y \sim \phi^n$) and the estimated fractal dimensions (D^* and D^{**} denote the values estimated, respectively, using m and n) with the concentration of nanofibers. The critical volume fractions of the I-to-II and II-to-III transitions are, respectively, 0.0068 and 0.034

	m	n	D^*	D^{**}
Regime I: entangled network	—	—	—	—
Regime II: aggregated network (strong-link regime)	2.1	1.8	—	1.9
Regime III: aggregated network (weak-link regime)	6.3	6.9	2.8	2.7

The latter network is considered to have a fractal nature where the aggregates (flocs) are closely packed throughout the sample. This fractal nature is related to the dependency of the rheological parameters G_0 and σ_y on the nanofiber concentration where two behaviors can be distinguished-depending on the strength of the interfloc links in comparison to that of the flocs (intrafloc) in the three-dimensional network: strong-link behavior (eqn (1)) and weak-link behavior (eqn (2)):[45,46]

$$G_0 \sim \phi^{(3+x)/(3-D)} \quad (1)$$

$$G_0 \sim \phi^{1/(3-D)} \quad (2)$$

where D is the fractal dimension of the flocs and x is the backbone fractal dimension of the flocs. In the strong-link regime, the interfloc links are stronger than the intrafloc links at low ϕ and the macroscopic elasticity is dominated by intralinks.[45,46] In this regime, the fractal dimension D cannot be calculated using the power-law exponent of G_0 predicted by the Shih model (eqn (1)) due to the unusual negative value of x.[47] Alternatively, D is calculated from the power law exponent of σ_y:[48,49]

$$\sigma_y \sim \phi^{2/(3-D)} \quad (3)$$

and was found to be 1.9 in accordance with the scaling model in the strong-link regime of flocculated suspensions.[45,46,50,51] This fractal dimension implies a fast aggregation when the flocs grow by merging into one another as soon as they collide (diffusion-limited aggregation, DLA[52,53]). As the nanofiber concentration increases, the suspensions are in the weak-link regime where the flocs are more rigid than the interfloc links so that the macroscopic elasticity of the interfloc links determines the elasticity of the suspensions.[45,46] The scaling relations of G_0 and σ_y (eqn (2) and (3)) show almost similar fractal dimension D = 2.7–2.8 in an excellent agreement with the predicted value in the weak-link regime.[46] This implies a different aggregation mechanism (reaction-limited aggregation, RLA) where the flocs penetrate to one another partially after collision[39] and a more compact structure[32] is formed in highly concentrated suspensions.

In conclusion, the CNF suspensions, below the rheological percolation threshold, are self-similar entangled networks that cannot be explained from the framework of the fractal network.[44] At the percolation threshold (ϕ_r^* = 0.0068), they exhibit a transition from DLA (D = 1.9) to RLA (D = 2.7) as the concentration increases in agreement with previous findings.[51] Such transition is in line with microstructural evolution of the aggregated suspensions that are large flocs linked by fibers (strong-link regime) and transform into a densely-packed (compact) network of more rigid flocs at higher concentration.

3.4. Electrical properties of CNF suspensions

Simultaneous measurements for the electric conductivity of the suspensions at no perturbation (after the dynamic frequency sweep) proved to be an efficient way to eliminate any additional stress and produce consistent interpretation for the microstructure of suspensions under investigation.[5,6] The degree of particles' agglomeration, extent of conductive pathways through the network and the electrical resistance of the gaps between particles/aggregates are reflected by the electric conductivity of the suspensions (Σ). Fig. 5 represents the variation of the impedance spectra (Fig. 5) with the volume fraction of CNFs. It can be seen that the dilute suspensions show a nearly linear Nyquist plot similar to that of the electrolyte (1 M LiTFSI in PC) implying the ionic nature of the suspensions. As the CNF concentration increases, typical semicircle Nyquist plots start to appear above a concentration threshold, the so-called electrical percolation threshold ϕ_e^*, indicating the build-up of the conductive network. This transition has been previously found in carbon black suspensions in the same electrolyte.[5]

Fig. 4a shows a quantitative variation of the electric conductivity with the volume fraction of CNFs. At low ϕ, the electric conductivity is nearly constant until the percolation threshold beyond which the electric conductivity sharply increases exhibiting a power-law relation:

$$\Sigma \sim \phi^l \quad (4)$$

with an exponent l = 2.5. This exponent is in agreement with the theoretical one (l = 2) reported for the three-dimensional percolating network[54] and experimental values (l = 2.2 and 2.3)

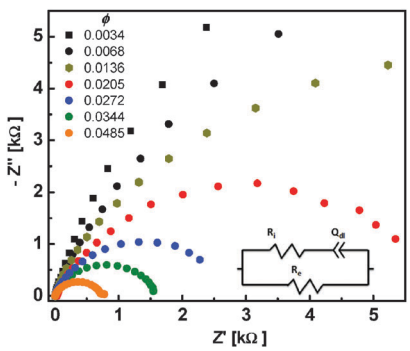

Fig. 5 Impedance spectra represented by Nyquist plots for CNF suspensions at various CNF concentrations (at 25 °C, 100 mV) measured in plate–plate geometry with a plate diameter of 50 mm and a gap of 1 mm. The equivalent circuit used in the analysis is superimposed on the Nyquist plot. The migration of the ions is described by an ionic resistor R_i associated in series with a capacitive element Q_{dl} to take into account the accumulation of ions at the surface of the electrodes compensating their polarization, known as the double-layer. The part of the circuit corresponding to the presence of nanofibers is placed in parallel with the ionic branch. It constituted a pure electronic resistance R_e to take into account the circulation of the electrons through the percolating network.[5]

found in CNT/polymer nanocomposites[55–58] and the 3D network of carbon black suspensions.[5]

Surprisingly, the electrical percolation threshold (ϕ_e*) coincides with the rheological threshold at a volume fraction of 0.0068. Some CNT/polymer nanocomposites showed coincidence thresholds[59–61] in contrast to the common behavior of flocculated suspensions where $\phi_e^* > \phi_r^*$.[55,56,62,63] It is well stated that the electrical percolation threshold is reached when the fibers approach each other with a few nm resulting in conductive pathways across the network. Therefore, the required fiber–fiber distance for electrical conductivity percolation is smaller than that for the rheological percolation, so that less nanofiber is required to reach the electrical conductivity threshold.[55] This is the situation for the entangled network of the nanofibers before the percolation threshold (0.0068) above which a superstructure of the aggregate-based network formed from aggregates (flocs) linked by nanofibers such that the conductive pathways are dominated. As the concentration increases, the flocs get densely packed leading to higher electrical conductivity. This trend is in accordance with the dynamic rheological data. However, the rheological behavior of the suspensions is likely to be more sensitive to the structural transition than their electrical behavior: the variation of the rheological parameters G_0 and σ_y (Fig. 4a and b) with ϕ presents two inflection points at ϕ = 0.0068 and 0.034, corresponding to a structural transition from the open fractal structure to densely-packed one.

In this study, we define the percolation threshold (ϕ = 0.0068) to be the volume fraction of CNFs at which the transition from the entangled to superstructure (aggregate-based) network occurs. However, even the entangled network possesses conductive pathways at ϕ = 0.00204 in accordance with CNTs.[61,64] In general, the flocculated suspensions commonly showed varied percolation thresholds and scaling exponents as a consequence of the formation process, particle size, interparticle interactions,[65,66] dispersing medium,[67] aspect ratio, and external stress (*e.g.* applied voltage).[61,62]

3.5. Steady shear rheology of CNF suspensions

The dynamic viscoelasticity and the simultaneous impedance spectra at rest revealed the development of the microstructure of suspensions with the concentration of the CNFs, at nearly no perturbation. Then, it is necessary to examine the effect of continuous shear flow on the microstructure of suspensions and account for any possible shear-induced structure/alignments in the internal structure.

Fig. 6 demonstrates the flow curves (steady shear viscosity η or shear stress σ *versus* the applied shear rate $\dot{\gamma}$), and a comparison between the dynamic complex viscosity η^* with the steady shear viscosity. First, the steady viscosity η increases with the concentration of nanofibers.[68] The suspension at low concentration (ϕ = 0.00136) exhibits a monotonic non-Newtonian shear-thinning behavior over the entire shear rate (Fig. 6a) in accordance with flocculated colloidal suspensions of CNFs[38] and CNTs.[31,36,40,41,69] Interestingly, the suspensions at $\phi \geq$ 0.00204 show a three-regime flow curve: two shear-thinning regions at low and high shear rates separated by a shear-thickening (or plateau) region over intermediate shear rates (Fig. 6a and b). Upon sweeping the shear rate forward and backward a minor hysteresis appears indicating the reversibility of shear thickening. The thickening region is modest at low concentration and becomes pronounced and shifts to a higher shear rate as the CNF concentration increases. Such behavior has been found in suspensions of spherical colloids[5,70] and anisometric CNTs.[69,71]

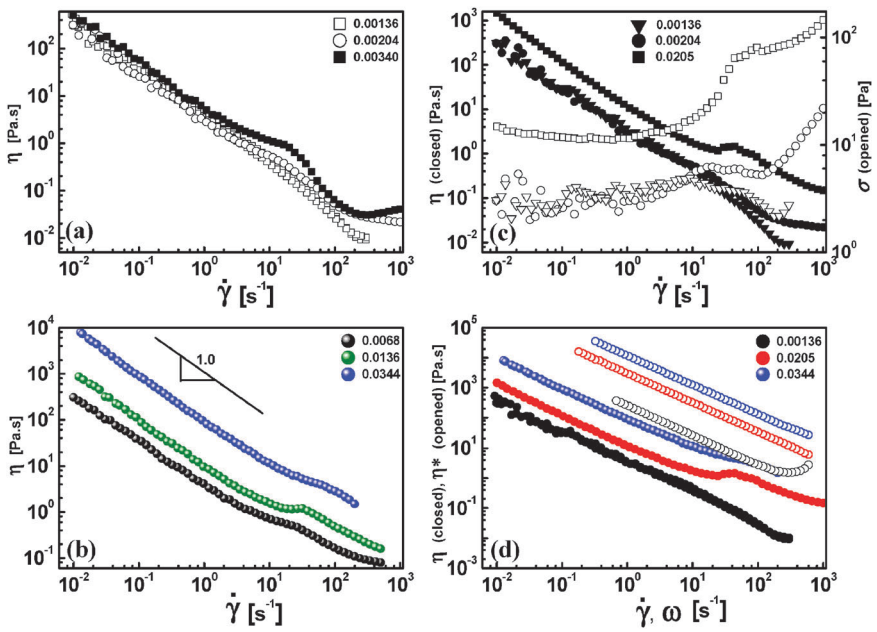

Fig. 6 Flow curves (a–c) and comparison between steady (η) and complex ($|\eta^*|$) viscosity (d) for CNF suspensions. The complex viscosity is extracted from the dynamic frequency sweep (linear) rheology.

In general, the low-shear rate viscosity (before the thickening region) obeys a power-law expression: $\eta \sim \dot{\gamma}^{-10}$, with a common exponent identical to the theoretical one[72] but independent of the CNF concentration. According to the orientation/aggregation model,[72] the interparticle interactions, hydrodynamic forces and network elasticity are the controlling forces for the rheological behavior of suspensions under shear flow. The relative importance of each force is dependent on the shear rate and particle concentration. The dilute suspension (at ϕ = 0.00136) is a simple entangled network of nanofibers (no aggregates) that align individually in the flow direction as a consequence of network breaking up due to shear flow[41] showing shear thinning over the entire shear rate range. As the CNF concentration increases, the network elasticity (due to agglomeration) and interparticle interactions become pronounced and the relative importance of each factor is concentration-dependent.[72] At low shear rates, the rod–rod interaction is dominant where the shear flow distorts the equilibrium isotropic orientation distribution of the fibers into anisotropic (ellipsoid) distribution[72] resulting in the shear-thinning (thinning I). On the other hand, the hydrodynamic forces are dominant at higher shear rates[72] leading to a higher degree of alignment of the nanofibers (thinning II).

The shear-thickening exhibited by the aggregate-based suspensions is likely to attribute to the formation of anisotropic aligned aggregates analogous to the hydroclusters formed in suspensions of spherical particles.[73,74] These anisotropic aggregates seem to erode resulting in higher effective volume fractions[75,76] and, hence, shear-thickening behavior at intermediate shear rates. Flow-induced agglomeration has been reported previously for CNT suspensions.[77,78] Interestingly, the suspensions well below the percolation threshold also exhibit mild shear-thickening indicating the onset of aggregation formation but the percolating network has not established yet. The shear thickening can be viewed as a steep jump in the shear stress with increasing shear rate as shown in Fig. 6c. This jump is steeper for the percolating suspension (ϕ = 0.0205) than for the non-percolating one (ϕ = 0.00204) implying the higher packing fraction of eroded aggregates analogous to the densely packed suspensions and colloids.[79] However, the entanglement-based suspension (ϕ = 0.00136) lacks the formation of anisotropic aggregates and only shows monotonic shear-thinning consistent with leveling-off the shear stress over the entire shear rate range.

The effect of continuous shear flow on the microstructure of suspensions can be seen when comparing the steady viscosity (η) with the complex viscosity ($|\eta^*|$) as depicted in Fig. 6d. For both diluted and concentrated suspensions, $|\eta^*|$ is one-decade higher than η at the same shear rate or frequency. This implies that the CNF suspensions do not obey the Cox–Mertz rule over the entire range of shear rate or frequency. Such behavior has been reported for suspensions of CNFs[38] and CNTs[41,69,80] when the network is established. Such deviation from the Cox–Mertz rule ($\eta < |\eta^*|$) is likely to be a consequence of the breaking of links between aggregates at the equilibrium (initial) state due to continuous shear flow.

3.6. Rheo-electrical behavior of CNF suspensions

Simultaneous measurements for the electric conductivity of the suspensions under continuous shear flow can elucidate the flow-induced structures or alignments that may be exhibited by the conductive suspensions of carbonaceous materials.[5,6,81]

The variation of the Nyquist plot shapes under shear flow is certainly a consequence of shear-induced structural transition. Therefore, it is necessary to quantitatively account for the variation of electric conductivity with the shear rates (Fig. 7d), as will be discussed below. This figure displays the conductivities of percolating suspensions by fitting the semicircles only by the proposed equivalent circuit, while the linear plots do not. Therefore, the rheo-electrical behavior of dilute and entangled suspensions will be discussed qualitatively.

In the quiescent state, the rheological and electrical behaviors of CNF suspensions revealed a percolation threshold (ϕ = 0.0068) that separates the entangled network from the percolating one. Far below this threshold, the diluted suspension at ϕ = 0.00136 shows a clear linear Nyquist plot at rest (0 s^{-1}) which does not change upon shearing the sample (from 0.01 to 1000 s^{-1}) (Fig. S3 in the ESI†). This suspension is purely ionic conductive and insensitive to the applied shear rate indicating a minor degree of entanglement for this CNF (aspect ratio $\sim$ 100) suspension[31] and hence, it lacks electrical pathways. This suspension exhibits a monotonic shear-thinning without a thickening region (Fig. 6a) implying the absence of any kind of agglomeration.

As the CNF concentration increases, the degree of entanglement become pronounced so that the entangled suspension at ϕ = 0.00204 shows a nearly semicircle plot (Fig. 7a) implying the onset of the growth of electrical pathways. Upon shearing the suspension from 0.1 s^{-1} to 100 s^{-1} the nearly semicircle plot continuously transforms into linear plots until approaching the linear plot of the electrolyte implying that the suspension is no longer conductive. Above the critical shear rate (100 s^{-1}), the Nyquist plots surprisingly approach the nearly semicircle plot of the quiescent state at 1000 s^{-1} (Fig. 7a), *i.e.* the conductivity tends again to increase. The decrease in the conductivity (below 100 s^{-1}) is likely due to the breaking up of small aggregates and a reduction in the degree of entanglement while the nanofibers align in the flow direction[82] in tandem with the shear-thinning behavior discussed above. Above 100 s^{-1}, the shear-induced anisotropy causes an increase in the conductivity in agreement with the behavior of CNT suspensions at high shear rates.[82]

On the other hand, the percolating suspension (ϕ = 0.0205) shows a typical semicircle Nyquist plot at rest (0 s^{-1}) which gets progressively wider upon shearing the suspension from 0.1 s^{-1} until a critical shear rate at 10 s^{-1}. Beyond this critical value, the semicircles again get narrower until approaching the semicircle of the suspension at rest (Fig. 7b). The simultaneous rheo-electrical behavior of the percolating suspensions is quantitatively depicted in Fig. 7c and d. In general, the conductivity of suspensions at rest rationally increases with the CNF concentration. Upon shearing the suspensions, the conductivity drops in tandem with the first shear-thinning region (thinning I) indicating the destruction of the percolating network into smaller agglomerates. The conductivity drop becomes less steep as the CNF concentration increases as a consequence of strong rod–rod interaction and probably relatively large agglomerates that still

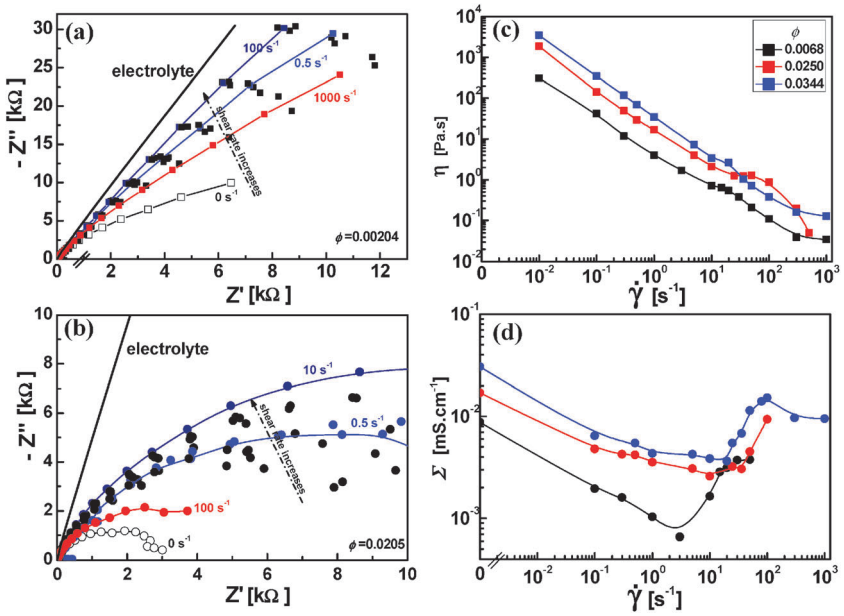

Fig. 7 The effect of shear rate on the electrical behavior of suspensions represented by Nyquist plots for (a) diluted suspension and (b) percolating suspension, and the variation of suspension's viscosity η (c) and electrical conductivity Σ (d) with the shear rate for percolating suspensions. Using the proposed equivalent circuit and EC-Labs software the semicircle plots only were fitted to obtain the conductivity values.

wire the network. Above a critical shear rate (depending on ϕ), the conductivity again rises consistent with the shear-thickening at higher intermediate shear rates as a result of the erosion between anisotropic aggregates that preserves the conductive pathways. At higher shear rates, the conductivity shows a mild increase in accordance with the second shear-thinning region (thinning II) where the aggregates break up and the density of effective aligned nanofibers increases. It is worth noting that the conductivity minimum becomes less pronounced and shift to higher (critical) shear rates as the nanofiber concentration increases. This presumably is a consequence of larger shear-induced aggregations with a considerable degree of anisotropy at higher CNF concentrations.

Such an inverted bell-like conductivity–shear rate curve has been reported for carbon black suspensions.[5] Various experimental[77,82,83] and numerical[84] studies on the conductivity of CNT/polymer suspensions under shear flow revealed the domination of the aggregation mechanism at low shear rates and the alignment mechanism at higher shear rates.

3.7. Comparison between CNF and CB suspensions and their mixture

The rheological and electrical properties of the suspensions of carbon materials were found to change with chemical properties and morphology of particles as well as the suspending medium.[5,85,86] Hence, the effect of particle morphology (carbon nanofibers *versus* carbon black; KB) on the rheological and electrical properties of their suspensions in the same suspending medium (1 M LiTFSI in PC) is worth examining.

The rheo-electrical properties of KB suspensions in 1 M LiTFSI in PC over a wide concentration range have been studied recently.[5] The KB suspensions showed a distinct transition from liquid-like ($G'' > G'$) to weak-gel viscoelastic ($G' > G''$)[5] where the KB network began to be constructed at ϕ = 0.002. This was defined as the rheological percolation threshold. Such transition is not obvious for CNF suspensions which show a gel-like response even at very low concentration due to their high aspect ratio. Therefore, the definition of rheological percolation threshold is varied and a quantitative comparison between the thresholds of KB and CNFs is not rational. However, it should be assumed that anisometric CNFs have lower rheological percolation threshold than isometric KB when the interconnected network is built up; *i.e.* when the viscoelastic behavior ($G' > G''$) appears. Comparatively, Fig. S4 in the ESI† depicts the variation of the rheological plateau modulus and electrical conductivity of CNFs and KB suspensions over a wide concentration range. In general, the CNF suspensions show a three-regime G_0–ϕ curve *versus* a monotonic increase of G_0 with the KB concentration (Fig. S4a, ESI†). This implies different mechanisms of structural evolution of CNFs and KB suspensions with the concentration. As described above, the CNFs exhibited a structural transition from the entangled state to the aggregate-based network which gets more compact as the nanofiber concentration increases. On the other hand, the KB suspensions are isolated agglomerates which grow with the KB concentration and eventually percolate.[5] Such different microstructures can be probed by following the power law exponents of $G_0 \sim \phi^m$, where m = 2.07 and 3.51 for CNFs and KB suspensions, respectively. These exponents are related to the fractal dimension D, where the percolated CNFs show D = 1.9 lower than that of the percolated network of KB (D = 2.5). Interestingly, these fractal dimensions indicate a common rapid (diffusion-limited) aggregation with the aggregate–aggregate aggregation mechanism for CNFs and particle–particle aggregation

for KB suspensions.[32] The lower the value of D, the more open is the floc structure; and hence the CNFs are likely to form less compact networks formed from large aggregates linked by nanofibers whereas, the relatively small KB aggregates form more dense networks. Different aggregation mechanisms and network compactness are consequences of different aspect ratios of the particles, where highly anisometric nanofibers (aspect ratio = 100) might produce a network with less packing fractions than that of isometric spherical carbon black (aspect ratio = 1) in accordance with the findings reported previously.[87]

Generally, the CNF suspensions have G_0 higher than that of the KB suspensions. Below ϕ = 0.0068 (the rheological percolation threshold of CNFs), the rigidity of highly entangled nanofibers is two-decade higher than that of loose and small KB aggregates. Above this concentration, G_0 of both suspensions approaches each other when both suspensions are quite percolated. It is the aggregate-based microstructure in which the larger CNF aggregates are linked by freely rotating nanofibers resulting in highly interacting flocs but still more open networks than relatively small KB aggregates that form more compact structures. Such differentiation in the microstructure is reflected in the rheological plateau modulus where it is likely that the large aggregates and connecting bundles of nanofibers show higher rigidity than that of smaller aggregates linked by relatively weak KB branches.

It should be noted that the electrical conductivity values of suspensions (CNFs or KB) were obtained by fitting the nearly or semicircle Nyquist plots by the proposed equivalent circuit in this study (see the caption of Fig. 5). As can be seen from Fig. S5 in the ESI†, the suspensions show nearly semicircle Nyquist plots at ϕ = 0.00204 for CNFs and ϕ = 0.0034 for KB. They are the critical concentrations at which the insulating suspensions transform into electrically conductive ones when the conductive pathways begin to be built through the suspensions. Therefore, it is worth mentioning that the CNFs are electrically percolated at a concentration nearly twice lower than that of KB. Similar to the rheological behavior, the electrical conductivity of the CNF suspensions remains constant at low CNF concentrations then suddenly increases above an obvious electrical percolation threshold (ϕ_e* = 0.0068) where the suspensions exhibit an entangled-to-aggregated transition (Fig. S4b, ESI†). However, the KB suspensions do not show such an inflection point which separates the insulating and conducting suspensions. The carbon particles' morphology and perhaps different surface chemistry are likely to be the main factors which result in varied percolation thresholds and microstructural transitions. As the carbon concentration increases, the anisometric nanofibers show insulating-to-conductive-to-fully percolated networks, in contrast to the isometric KB which exhibits insulating-to-percolated suspensions.

For the fully percolated KB and CNF suspensions, the electrical conductivity shows a power-law relation: $\Sigma \sim \phi^l$, with different exponents: l = 1.83 and 2.47 for KB and CNFs, respectively. These exponents fall in the theoretical range reported for 2D and ideal 3D networks,[54] where l = 2.47 is consistent with a 3D network of aggregated CNFs while l = 1.83 suggests KB arranged in a 2D network.[5] This difference is likely attributed to the varied particle size and morphology where a denser network allows almost 2D conducting paths in agreement with the trend of the plateau modulus.

In contrast to the rheological behavior, CNF suspensions are less conductive than the KB suspensions under the same conditions (Fig. S4b, ESI†). This behavior may be linked to different mechanisms of structural evolution between nanofibers and carbon black suspensions, where most of the electric current is lost in the inner fibers and the electric current only flows on the outermost fibers in bundled CNFs.[11]

4. Suspensions of mixed carbons

In addition to enhancing the mechanical properties of polymer-based composites, mixtures of carbonaceous materials (*e.g.* carbon black and nanotubes) have been used to increase the electrical conductivity of the composites.[88–90] Little research has been done in this area and we found a necessity to examine the effect of nanofibers on the rheo-electrical properties of carbon black suspensions. Fig. 8 presents the rheo-electrical properties of examples of suspensions composed of varied mixtures of CNFs and KB at a total concentration fixed at 2 wt% (ϕ = 0.0136). As can be seen from Fig. 8a, the replacement of up to 1 wt% KB by an equivalent amount of CNFs does not significantly alter the network rigidity but increases the electrical conductivity of the suspensions. Further increasing the CNF ratio results in an increase in the rigidity and dramatically decreases the conductivity of the suspension. This behavior can be explained on the basis of the formation of a co-supporting network[88,89] of randomly distributed nanofibers and KB particulates where the nanofibers, at low content, act as long-distance wires and the particulate KB forms local conductive paths acting as interconnections between the nanofibers. At higher CNF ratio, the presence of aggregated nanofibers seems to break up the KB branches and then the hybrid suspensions lose their electrical conductivity.

Fig. 8b displays the variation of electrical conductivity of the suspensions of KB–CNF mixed carbons under shear flow. It can be seen that the conductivity–shear rate curves have an inverted bell-like shape with pronounced minima in accordance with a previous study.[5] This trend is linked to a structural transition under shear flow where the network of highly structured suspensions breaks up at low shear rates so that the conductivity drops then the formation of large anisometric aggregates (at moderate shear rates) and small aggregates with high density of effective chains (at higher shear rates) again increases the conductivity of suspensions.[5] However, the suspension at 0.5 wt% CNFs + 1.5 wt% KB shows conductivity nearly independent of the shear rate. This may imply that the flexible ''non-aggregated'' nanofibers, at a small amount of CNFs, simply wires the broken KB aggregates under flow[6] so that the conductivity does not alter in contrast to suspensions at higher CNF content (1 wt%) where the aggregated nanofibers show a synergetic effect with the KB aggregates which are sensitive to shear flow.

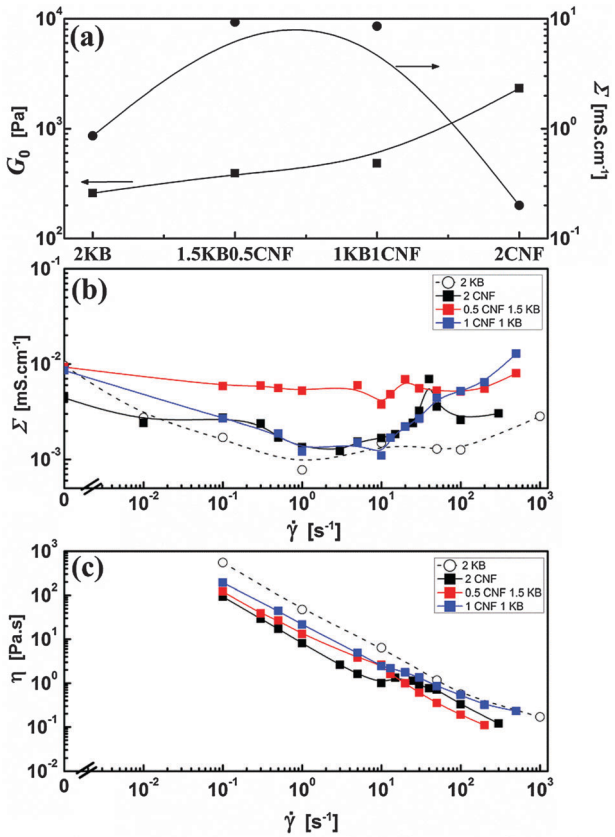

Fig. 8 Rheological and rheo-electrical properties of CNF–KB mixed carbons represented by the variation of plateau modulus and electrical conductivity with the carbon concentration (a), and the effect of the shear rate on the steady shear viscosity (b) and electrical conductivity of the suspensions (c). The concentration of carbon materials is represented by wt% (*e.g.* 1.5KB0.5CNF denotes 1.5 wt% KB and 0.5 wt% CNFs, *etc.*).

The shear-induced structural transition can also be interpreted from the steady viscosity–shear rate curves as depicted in Fig. 8c. Except for the 2 wt% KB,[91] the suspensions exhibit three-regime flow curves: two shear-thinning regimes at low and high shear rates separated with the shear-thickening region at moderate shear rates in agreement with reported systems.[5,6,75,92] Such a thickening region is more pronounced for pure 2 wt% CNFs and gradually diminishes as the KB ratio increases suggesting that the shape and size of aggregates are closely connected with the overall flow behavior of the suspensions.

5. Conclusion

The rheo-electrical measurements efficiently accounted for the equilibrium microstructure and shear-induced transition exhibited by suspensions of carbon nanofibers (CNFs) in an organic electrolyte (1 M lithium bis(trifluoromethanesulfonamide) in propylene carbonate). Such nonaqueous conductive suspensions are precursor formulation for electrodes in energy storage systems such as redox flow batteries.

Over a wide range of CNF concentration, the suspensions commonly exhibited a gel-like viscoelastic response coinciding with rheological and electrical percolation threshold at ϕ = 0.0068. This threshold separates two different networks: entangled- and aggregate-based structures controlled, respectively, by diffusion-limited aggregation (DLA) and reaction-limited aggregation (RLA) mechanisms. Both types of networks showed a three-regime flow curve (viscosity *vs.* shear rate) in agreement with the inverted-bell-like conductivity curve (electric conductivity *vs.* shear rate) indicating shear-induced alignments (for the entangled network) and structural (for the aggregated network) transitions.

Owing to different particle morphologies and hence aggregation mechanisms, the suspensions of anisometric CNFs showed higher rigidity than those of isometric carbon black (CB) in the same electrolyte. In contrast, the CB suspensions presented higher electric conductivity than that of their analogous CNFs as a consequence of the aggregate-based network of the CNFs where the electric current likely only flows in the outermost linked fibers rather than the aggregates (bundles). A hybrid suspension of CNFs and CB at an optimum mixing ratio resulted in enhanced electric conductivity with nearly no influence on the suspension rigidity and on their electric conductivity under shear flow.

References

1 K. Tatsumi, K. Zaghib, Y. Sawada, H. Abe and T. Ohsaki, *J. Electrochem. Soc.*, 1995, **142**, 1090.
2 J. Liu, K. Tang, K. Song, P. A. van Aken, Y. Yu and J. Maier, *Phys. Chem. Chem. Phys.*, 2013, **15**, 20813.
3 M. Endo, Y. A. Kim, T. Hayashi, K. Nishimura, T. Matusita, K. Miyashita and M. S. Dresselhaus, *Carbon*, 2001, **39**, 1287.
4 C. Kim, K. S. Yang, M. Kojima, K. Yoshida, Y. J. Kim, Y. A. Kim and M. Endo, *Adv. Funct. Mater.*, 2006, **16**, 2393.
5 M. Youssry, L. Madec, P. Soudan, M. Cerbelaud, D. Guyomard and B. Lestriez, *Phys. Chem. Chem. Phys.*, 2013, **15**, 14476.
6 M. Youssry, L. Madec, P. Soudan, M. Cerbelaud, D. Guyomard and B. Lestriez, *J. Power Sources*, 2015, **274**, 424.
7 M. Inagaki, H. Konno and O. Tanaike, *J. Power Sources*, 2010, **195**, 7880.
8 A. V. Melechko, V. I. Merkulov, T. E. McKnight, M. A. Guillorn, K. L. Klein, D. H. Lowndes and M. L. Simpson, *J. Appl. Phys.*, 2005, **97**, 041301.
9 B. K. Ku, M. S. Emery, A. D. Maynard, M. R. Stolzenburg and P. H. McMurry, *Nanotechnology*, 2006, **17**, 3613.
10 L. A. Girifalco, M. Hodak and R. S. Lee, *Phys. Rev. B: Condens. Matter Mater. Phys.*, 2000, **62**, 13104.
11 H. Stahl, J. Appenzeller, R. Martel, P. Avouris and B. Lengeler, *Phys. Rev. Lett.*, 2000, **85**, 5186.
12 B. Vigolo, A. Pénicaud, C. Coulon, C. Sauder, R. Pailler, C. Journet, P. Bernier and P. Poulin, *Science*, 2000, **290**, 1331.
13 V. C. Moore, M. S. Strano, E. H. Haroz, R. H. Hauge, R. E. Smalley, J. Schmidt and Y. Talmon, *Nano Lett.*, 2003, **3**, 1379.

14 L. Calvillo, M. J. Lázaro, I. Suelves, Y. Echegoyen, E. G. Bordejé and R. Moliner, *J. Nanosci. Nanotechnol.*, 2009, **9**, 4164.
15 N. T. Hung, N. M. Tuong and E. G. Rakov, *Inorg. Mater.*, 2010, **46**, 1077.
16 V. Datsyuk, M. Kalyva, K. Papagelis, J. Parthenios, D. Tasis, A. Siokou, I. Kallitsis and C. Galiotis, *Carbon*, 2008, **46**, 833.
17 K. Shen, H. Xu, Y. Jiang and T. Pietraß, *Carbon*, 2004, **42**, 2315.
18 S. C. Mun, M. Kim, K. Prakashan, H. J. Jung, Y. Son and O. O. Park, *Carbon*, 2014, **67**, 64.
19 A. Celzard, E. McRae, C. Deleuze, M. Dufort, G. Furdin and J. F. Marêché, *Phys. Rev. B: Condens. Matter Mater. Phys.*, 1996, **53**, 6209.
20 C. Penu, G.-H. Hu, A. Fernandez, P. Marchal and L. Choplin, *Polym. Eng. Sci.*, 2012, **52**, 2173.
21 J. N. Coleman, S. Curran, A. B. Dalton, A. P. Davey, B. McCarthy, W. Blau and R. C. Barklie, *Phys. Rev. B: Condens. Matter Mater. Phys.*, 1998, **58**, R7492.
22 L. Madec, M. Youssry, M. Cerbelaud, P. Soudan, D. Guyomard and B. Lestriez, *J. Electrochem. Soc.*, 2014, **161**, A693.
23 E. Anczurowski, R. G. Cox and S. G. Mason, *J. Colloid Interface Sci.*, 1967, **23**, 533.
24 M. H. Al-Saleh and U. Sundararaj, *Carbon*, 2009, **47**, 2.
25 K. Hyun, S. H. Kim, K. H. Ahn and S. J. Lee, *J. Non-Newtonian Fluid Mech.*, 2002, **107**, 51.
26 M. Youssry, L. Coppola, I. Nicotera and C. Morán, *J. Colloid Interface Sci.*, 2008, **321**, 459.
27 I. A. Kinloch, S. A. Roberts and A. H. Windle, *Polymer*, 2002, **43**, 7483.
28 L. A. Hough, M. F. Islam, P. A. Janmey and A. G. Yodh, *Phys. Rev. Lett.*, 2004, **93**, 168102.
29 F. C. MacKintosh, J. Käs and P. A. Janmey, *Phys. Rev. Lett.*, 1995, **75**, 4425.
30 R. Tharmann, M. M. A. E. Claessens and A. R. Bausch, *Phys. Rev. Lett.*, 2007, **98**, 088103.
31 S. S. Rahatekar, K. K. Koziol, S. R. Kline, E. K. Hobbie, J. W. Gilman and A. H. Windle, *Adv. Mater.*, 2009, **21**, 874.
32 Th. F. Tadros, *Rheology of Dispersions: Principles and Applications*, Wiley-VCH Verlag GmbH & Co. KGaA, Weinheim, 2010.
33 M. Kawaguchi, M. Okuno and T. Kato, *Langmuir*, 2001, **17**, 6041.
34 V. Grenard, N. Taberlet and S. Manneville, *Soft Matter*, 2011, **7**, 3920.
35 E. K. Hobbie and D. J. Fry, *J. Chem. Phys.*, 2007, **126**, 124907.
36 K. M. Yearsley, M. R. Mackley, F. Chinesta and A. Leygue, *J. Rheol.*, 2012, **56**, 1465.
37 E. E. Urenà-Benavides, M. J. Kayatin and V. A. Davis, *Macromolecules*, 2013, **46**, 1642.
38 J. Xu, S. Chatterjee, K. W. Koelling, Y. Wang and S. E. Bechtel, *Rheol. Acta*, 2005, **44**, 537.
39 R. Larson, *The Structure and Rheology of Complex Fluids*, Oxford University Press, 1999.
40 A. W. K. Ma, M. R. Mackley and F. Chinesta, *Int. J. Mater. Form.*, 2008, **1**, 75.
41 Z. H. Fan and S. G. Advani, *J. Rheol.*, 2007, **51**, 585.
42 M.-C. Yang, L. E. Scriven and C. W. Macosko, *J. Rheol.*, 1986, **30**, 1015.
43 O. Lieleg, M. M. A. E. Claessens, C. Heussinger, E. Frey and A. R. Bausch, *Phys. Rev. Lett.*, 2007, **99**, 088102.
44 S. Marceau, Ph. Dubois, R. Fulchiron and Ph. Cassagnau, *Macromolecules*, 2009, **42**, 1433.
45 W.-H. Shih, W. Y. Shih, S.-I. Kim, J. Liu and I. A. Aksay, *Phys. Rev. A: At., Mol., Opt. Phys.*, 1990, **42**, 4772.
46 H. Wu and M. Morbidelli, *Langmuir*, 2001, **17**, 1030.
47 In the strong-link regime, D is expected to fall in the range of 1.7–2.0.[46] According to the exponent of G_0 the power law relation (eqn (1)) will yield negative x values ($x = -0.27$ and -0.90) which cannot be explained by the scaling model[45] and has been found in some colloidal suspensions[49].
48 F. Khalkhal, P. J. Carreau and G. Ausias, *J. Rheol.*, 2011, **55**, 153.
49 F. Khalkhal and P. J. Carreau, *Rheol. Acta*, 2011, **50**, 717.
50 N. B. Uriev and I. Y. Ladyzhinsky, *Colloids Surf., A*, 1996, **108**, 1.
51 K.-M. Jäger and D. H. McQueen, *Polymer*, 2001, **42**, 9575.
52 P. Meakin, *Phys. Rev. Lett.*, 1983, **51**, 1119.
53 M. Kolb, R. Botet and R. Jullien, *Phys. Rev. Lett.*, 1983, **51**, 1123.
54 D. Stauffer and A. Aharony, *Introduction to Percolation Theory*, Taylor & Francis, London, 1994.
55 F. Du, R. C. Scogna, W. Zhou, S. Brand, J. E. Fischer and K. I. Winey, *Macromolecules*, 2004, **37**, 9048.
56 G. Hu, C. Zhao, S. Zhang, M. Yang and Z. Wang, *Polymer*, 2006, **47**, 480.
57 F. M. Blighe, Y. R. Hernandez, W. J. Blau and J. N. Coleman, *Adv. Mater.*, 2007, **19**, 4443.
58 I. Alig, T. Skipa, D. Lellinger and P. Pötschke, *Polymer*, 2008, **49**, 3524.
59 O. Meincke, D. Kaempfer, H. Weickmann, C. Friedrich, M. Vathauer and H. Warth, *Polymer*, 2004, **45**, 739.
60 Q. Zhang, D. R. Lippits and S. Rastogi, *Macromolecules*, 2006, **39**, 658.
61 J. Sumfleth, S. T. Buschhorn and K. Schulte, *J. Mater. Sci.*, 2011, **46**, 659.
62 M. D. Lima, M. J. Andrade, V. Skakalova, C. P. Bergmann and S. Roth, *J. Mater. Chem.*, 2007, **17**, 4846.
63 C. Penu, G.-H. Hu, A. Fernandez, Ph. Marchal and L. Choplin, *Polym. Eng. Sci.*, 2012, **52**, 2173.
64 V. Skakalova, U. Dettlaff-Weglikowska and S. Roth, *Synth. Met.*, 2005, **152**, 349.
65 S. Mall and W. B. Russel, *J. Rheol.*, 1987, **31**, 651.
66 T. Amari and K. Watanabe, *J. Rheol.*, 1990, **34**, 207.
67 L. Vaisman, H. D. Wagner and G. Marom, *Adv. Colloid Interface Sci.*, 2006, **128–130**, 37.
68 In tandem with the variation of G_0 and σ_y with the nanofiber volume fraction (Fig. 4), the steady viscosity η (at 0.1 s^{-1}) similarly shows three-regime dependence of the volume fraction with different exponents indicating different microstructures. (Fig. S2, ESI†).

69 V. A. Davis, L. M. Ericson, A. N. G. Parra-Vasquez, H. Fan, Y. Wang, V. Prieto, J. A. Longoria, S. Ramesh, R. K. Saini, C. Kittrell, W. E. Billups, W. W. Adams, R. H. Hauge, R. E. Smalley and M. Pasquali, *Macromolecules*, 2004, **37**, 154.
70 A. Zaccone, D. Gentili, H. Wu, M. Morbidelli and E. Del Gado, *Phys. Rev. Lett.*, 2011, **106**, 138301.
71 X. Sha, K. Yu, H. Cao and K. Qian, *J. Nanopart. Res.*, 2013, **15**, 1816.
72 G. Natale, M. C. Heuzey, P. J. Carreau, G. Ausias and J. Férec, *AIChE J.*, 2014, **60**, 1476.
73 N. J. Wagner and J. F. Brady, *Phys. Today*, 2009, **62**, 27.
74 D. P. Kalman and N. J. Wagner, *Rheol. Acta*, 2009, **48**, 897.
75 C. O. Osuji, C. Kim and D. A. Weitz, *Phys. Rev. E: Stat., Nonlinear, Soft Matter Phys.*, 2008, **77**, 060402.
76 A. S. Negi and C. O. Osuji, *Rheol. Acta*, 2009, **48**, 871.
77 S. Lin-Gibson, J. A. Pathak, E. A. Grulke, H. Wang and E. K. Hobbie, *Phys. Rev. Lett.*, 2004, **92**, 048302.
78 E. K. Hobbie, *Rheol. Acta*, 2010, **49**, 323.
79 E. Brown and H. M. Jaeger, *J. Rheol.*, 2012, **56**, 875.
80 K. L. White, P. Li, Y. Sumi and H.-J. Sue, *J. Phys. Chem. B*, 2014, **118**, 362.
81 L. Madec, M. Youssry, M. Cerbelaud, P. Soudan, D. Guyomard and B. Lestriez, *ChemPlusChem*, 2015, **80**, 396.
82 S. Pujari, S. S. Rahatekar, J. W. Gilman, K. K. Koziol, A. H. Windle and W. R. Burghardt, *J. Chem. Phys.*, 2009, **130**, 214903.
83 S. B. Kharchenko, J. F. Douglas, J. Obrzut, E. A. Grulke and K. B. Migleri, *Nat. Mater.*, 2004, **3**, 564.
84 A. E. Eken, E. J. Tozzi, D. J. Klingenberg and W. Bauhofer, *Polymer*, 2011, **52**, 5178.
85 Y. Aoki, A. Hatano and H. Watanabe, *Rheol. Acta*, 2003, **42**, 209.
86 C. L. Barrie, P. C. Griffiths, R. J. Abbott, I. Grillo, E. Kudryashov and C. Smyth, *J. Colloid Interface Sci.*, 2004, **272**, 210.
87 T. Kitano, T. Kataoka and T. Shirota, *Rheol. Acta*, 1981, **20**, 207.
88 L. M. Clingerman, E. H. Weber, J. A. King and K. H. Schulz, *Polym. Compos.*, 2002, **23**, 911.
89 W. Thongruang, R. J. Spontak and C. M. Balik, *Polymer*, 2002, **43**, 2279.
90 M. Drubetski, A. Siegmann and M. Nakis, *J. Mater. Sci.*, 2007, **42**, 1.
91 The 2 wt% KB suspension does not show a clear shear-thickening region due to the formation of small and somewhat monodisperse hydroclusters which interact strong enough to have a higher yield stress[5] leading to masking the shear-thickening [E. Brown, N. A. Forman, C. S. Orellana, H. Zhang, B. W. Maynor, D. E. Betts, J. M. DeSimone and H. M. Jaeger, *Nat. Mater.*, 2010, **9**, 220].
92 B. J. Maranzano and N. J. Wagner, *J. Chem. Phys.*, 2001, **114**, 10514.